AIMS Energy, 13(6): 1391–1416.
DOI: 10.3934/energy.2025052
Received: 25 July 2025
Revised: 31 October 2025
Accepted: 13 November 2025
Published: 24 November 2025

https://www.aimspress.com/journal/energy

Research article

Numerical analysis of how azimuthally non-uniform heat flux influences turbulent convective heat transfer in parabolic trough solar collector

Hamzeh Jamali*

Department of Mechanical and Aerospace Engineering, Shiraz University of Technology, Shiraz, Iran. Official address: Iranian Ports and Maritime Organization (PMO), Bushehr, Iran.

* **Correspondence:** Email: xh.jxjamali@yahoo.com; Tel: +989177754752.

Abstract: In the present study, a 3D steady-state numerical analysis was performed to investigate forced convection heat transfer within a horizontal smooth tube carrying a heat transfer fluid (HTF) (a thermal oil, in this analysis) with turbulent flow and azimuthally non-uniform heat flux (NUHF). The effect of heat flux non-uniformity on the average Nusselt number, in relation to tube material conductivity and thickness, was examined through a conjugate heat transfer analysis. The analysis was conducted using the *SST* $k-\omega$ turbulence model for a Reynolds number ranges from 10,000 to 110,000, and fluid Prandtl numbers of 7.25, 0.3566, and 15.74, reflecting possible operating temperatures, in ANSYS Fluent software 18.2. A comparison was made between the average Nusselt number for various azimuthally NUHF distributions and for an azimuthally uniform heat flux (UHF). Subsequently, the effect of tube material conductivity and thickness on the average Nusselt number under azimuthally NUHF distribution was numerically investigated. The results show that the deviation of the Nusselt number with NUHF from that with UHF can exceed 84%. The findings specifically prove and highlight that the assumption of azimuthal heat flux uniformity on an absorber tube of a parabolic trough solar collector, made by many researchers, may lead to significant inaccuracies.

Keywords: convective heat transfer; heat flux; horizontal tube; parabolic trough solar collector; Nusselt number; turbulent flow

Nomenclature: C: coefficient; D: tube diameter (m); Gr: Grashof number; h: convective heat transfer coefficient; k: turbulent kinetic energy; Nu: Nusselt number; p: pressure; Pr: Prandtl number; q'': heat flux (W/m^2); Re: Reynolds number; Ri: Richardson number; u: velocity; v: velocity
Greek symbols: α: thermal diffusivity, exponent; ε: turbulent dissipation; θ: azimuthal angle of insulation (°); μ: dynamic viscosity; ν: kinematic viscosity; ρ: density; ω: specific turbulent dissipation rate (turbulence frequency)
Subscripts and superscripts: D: diameter; k: turbulent kinetic energy; nu: non-uniform heat flux; t: turbulent; u: uniform heat flux; ω: specific turbulent dissipation rate
Abbreviations: CFD: computational fluid dynamics; HTF: heat transfer fluid; *Ins.*: insulated; LCR: local concentration ratio; $NUHF$: non-uniform heat flux; $PTSC$: parabolic trough solar collector; $RANS$: Reynolds-averaged Navier-Stokes; $REAL$: realizable; RNG: renormalization groups; SST: shear stress transport; STD: standard; UHF: uniform heat flux

1. Introduction

Analyses of convective heat transfer in tubes have always been of great interest to scientists and technologists, considering factors such as boundary conditions, fluid type, flow regime, and the tube size and position (horizontal, vertical, or inclined). Due to the wide range of applications for horizontal fluid-carrying tubes, such as in the parabolic trough solar collector (PTSC) industry, it has become critically important for scientists to investigate horizontal tubes under various thermal and hydrodynamic conditions. PTSCs (Figure 1), as a sustainable and environmentally friendly means of clean electricity production [1], stand out among other clean and renewable energy technologies as one of the most promising alternatives to pollution-inducing industries, such as those driven by fossil fuels (where "every gas flare is a super heater against climate"), contributing to global warming. The absorber tube of a PTSC, as a typical example of a horizontal tube subjected to azimuthally non-uniform solar heat flux, is the primary focus of the current research. An absorber tube, which carries a heat transfer fluid, is positioned at the focal line of the PTSC's reflecting mirror [1]. As a result, the bottom part of the absorber tube experiences higher concentrated solar irradiation from the reflecting mirror, while the top part is only exposed to direct solar irradiation. This phenomenon clearly illustrates the non-uniform azimuthal solar heat flux around the absorber tube. A substantial number of studies have investigated the thermal efficiency of PTSCs using numerical [2–4], experimental [5–7], and analytical and theoretical [8–10] methods. In many numerical and nearly all analytical and theoretical analyses, the thermal behavior of PTSC absorber tubes has been evaluated based on the assumption of UHF distribution for the sake of calculation simplification [11–13]. Consequently, conventional correlations, such as the Dittus-Boelter equation, have been employed to calculate the Nusselt number [8,14–16]. However, in most numerical analyses, the specific effects of azimuthally NUHF on the Nusselt number and the convective heat transfer coefficient have been taken into account. Equation (1) represents the general definition of the Nusselt number, which relates the Nusselt number to the convective heat transfer coefficient of the fluid [17]:

$$Nu = \frac{hD}{k} \tag{1}$$

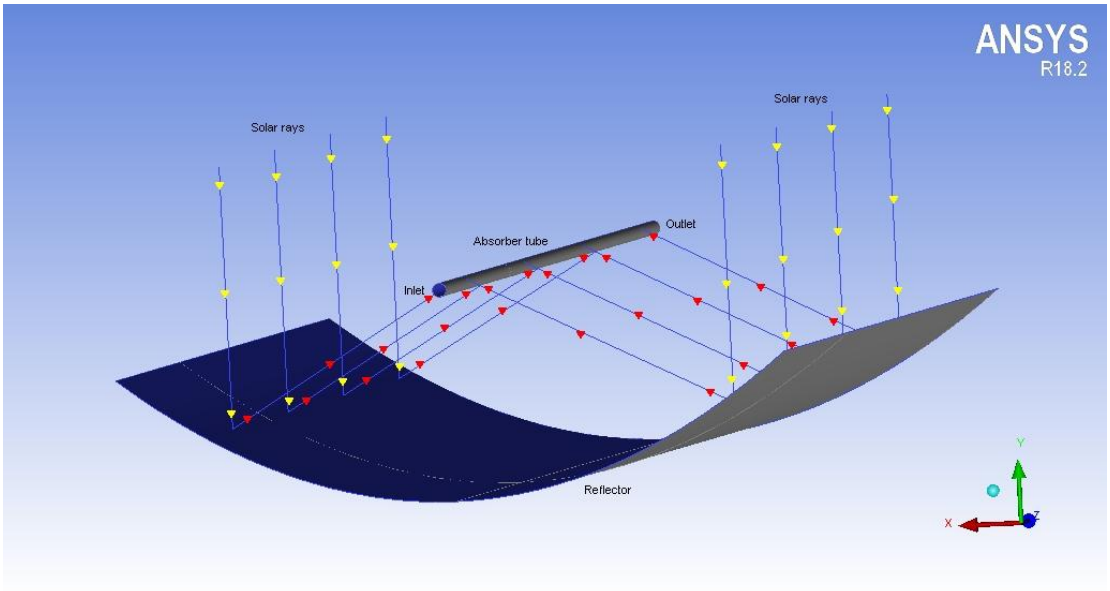

Figure 1. Schematic view of a parabolic trough solar collector (PTSC).

The effect of solar heat flux non-uniformity on the thermal efficiency of PTSCs is so considerable that some works not only considered this effect but also suggested the application of a rotating absorber tube to decrease it and consequently increase PTSC thermal efficiency [18–21]. The critical question raised here is how much error arises from the spurious assumption of solar heat flux uniformity in calculating the thermal efficiency of PTSCs. As is the aim of the current study, various researchers have already analyzed horizontal fluid-carrying tubes under different thermal boundary conditions. Adebiyi and Hall [22] launched an experimental analysis into heat transfer to supercritical and subcritical pressure CO_2 flowing through a uniformly heated horizontal pipe, within a Reynolds number range of 2×10^4 to 2×10^5. The results showed that, due to buoyancy effect, considerable decreases and increases in heat transfer are observed at the upper part and the lower part of the pipe, respectively, compared with the data in which buoyancy effects are not considered. Ghajar and Tam [23] investigated local and mixed convective heat transfer in a horizontal tube, within the Reynolds number range from 280 to 49,000, Prandtl number range from 4 to 158, and Grashof number range from 1000 to 2.5×10^5, regarding three inlet shape types, i.e., reentrant, bell-mouth, and square-edged inlets. The main results indicated that the secondary flow establishment, the heat transfer coefficient, and the heat transfer transition regions and boundaries were all strongly inlet-dependent. The correlation for fully-developed forced convection in the transition and turbulent regions for a bell-mouth inlet was in excellent agreement with the classical correlations developed by Gnielinski [24] and Churchill [25]. However, neither of the above-mentioned classical correlations were able to predict the mixed convection for the entrance and fully developed flows in the laminar and transition regions, regarding the inlet configurations. Boufendi and Afrid [26] conducted a numerical analysis of mixed convection in a uniformly heated horizontal pipe under various Grashof numbers and constant Prandtl and

Reynolds numbers (Pr = 3.02 and Re = 1000). The results showed that the local axial Nusselt number decreases along the entrance region and increases downstream. Mohammed and Salman [27] experimentally investigated mixed convection in a uniformly heated horizontal circular cylinder with hydrodynamically fully developed, thermally developing, and thermally developed laminar air flow, regarding various entrance sections. The results showed that for all entrance sections, the Nusselt number increases as the UHF increases. In the same year, Grassi and Testi [28] performed a study on mixed convection in the entry region of a uniformly heated horizontal cylindrical pipe with a weakly turbulent flow of perfluorohexane. The results showed that at the lower region, at a fixed flow rate and heat, the Nusselt number decreased in the developing flow region along the pipe and remained almost the same in the developed flow region, while at the upper region, the Nusselt number decreased along the aforementioned distance, with a developing flow region for the upper part. About one year later, Mohammed and Salman [29] performed an experimental study on hydrodynamically fully developed and thermally developing laminar free and forced convection in a uniformly heated horizontal tube, with Reynolds numbers ranging from 400 to 1600, UHF ranging from 60 W/m^2 to 400 W/m^2, and Richardson numbers ranging from 0.13 to 7.125. It was concluded that, for the same heat flux and high Reynolds number, the local Nusselt number, in forced convection domination, is lower than that pure forced convection, and vice versa due to natural convection domination. Testi [30] conducted a numerical analysis of transitional mixed convection in a uniformly heated horizontal cylindrical pipe with developing flow of FC-72. Heat transfer measurements were taken at various cross-sections along the tube. The difference between the Nusselt numbers at the top and bottom sides was more evident at higher Grashof numbers, lower Reynolds numbers, and higher $^{x}/_{D}$. Chae and Chung [31] experimentally investigated mixed convection in uniformly-heated horizontal pipes for Grashof numbers from 1.4×10^6 to 2.6×10^6, Reynolds numbers from 58 to 1270, and a fixed Prandtl number of 2094. The experimental results agreed well with the existing theoretical correlations for mixed convection, showing that the Nusselt numbers from the top half and the bottom half of the pipe were different due to the different thermal stratification caused by the secondary flow. Faheem et al. [11] performed a numerical study on turbulent mixed convection of air flow in uniformly heated smooth horizontal pipes with Reynolds and Richardson numbers of 2300 and 1.04, respectively. They utilized five RANS turbulence models available in ANSYS Fluent: STD $k-\varepsilon$, REAL $k-\varepsilon$, RNG $k-\varepsilon$, STD $k-\omega$, and SST $k-\omega$ models. STD $k-\varepsilon$ and REAL $k-\varepsilon$ models yielded more accurate results in predicting the Nusselt number and temperature in the inner region of the pipe.

Several studies have also investigated the effect of azimuthally NUHF in various heat transfer analyses in tubes, a few of which, inter alia, have already focused on the heat transfer analysis of a horizontal fluid-carrying tube with turbulent flow, examining the effect of azimuthal heat flux non-uniformity on convective heat transfer. Reynolds [32] conducted analytical research into turbulent heat transfer in a tube with variable azimuthal heat flux. The research was specifically based on a low Prandtl number turbulent (gas) flow with isotropic heat transfer. The results revealed that the effects of azimuthally NUHF in turbulent flow are considerable and more prominent than those in laminar flow, particularly at low Prandtl numbers. Black and Sparrow [33] experimentally investigated turbulent heat transfer in a tube with azimuthally non-uniform temperature and wall heat flux. Their experimental and analytical results on the average Nusselt number were in strong agreement with each other. The results were also close to those predicted by the Dittus-Boelter equation, though not in

complete agreement. Schmidt and Sparrow [34] performed an experimental study on turbulent flow of water in a horizontal tube with azimuthally NUHF, for Reynolds numbers ranging from 3,000 to 70,000 and varying Prandtl numbers from 3.5 to 11.5, with and without considering buoyancy effect. The results demonstrated that bottom heating significantly induced buoyancy effect at low Prandtl numbers, while the top-heated experiments were not affected by buoyancy. Additionally, substantial azimuthal variations of the Nusselt number and the wall temperature occurred in low-Reynolds-number, buoyancy-unaffected turbulent flows, while buoyancy-affected flows tended to increase azimuthal uniformity due to the existence of secondary flow. About one year later, Knowles and Sparrow [35] conducted experiments on heat transfer in an asymmetrically heated tube with turbulent airflow, within Reynolds numbers from 4,400 to 64,000. The results showed that, at low Reynolds numbers, the Nusselt number agreed well with that for uniform heating conditions (i.e., Dittus-Boelter and Petukhov-Popov correlations). However, at higher Reynolds numbers, azimuthal variations of the Nusselt number increased due to the effect of azimuthal conduction in the tube wall. It is noteworthy that the tendency toward greater non-uniformity due to increasing Reynolds number, in spite of the tendency toward heat flux uniformity due to the tube wall conduction, in the above-mentioned airflow, is contrary to the trend observed in experiments with water flow, such as the one Schmidt and Sparrow [34] performed. In the same year, Chieng and Launder [36] performed a numerical simulation of turbulent transport in flow through an asymmetrically heated pipe. They took into consideration the anisotropy of turbulent thermal diffusivities, regarding Black and Sparrow's study. The results revealed that the azimuthal variation of the Nusselt number diminishes as the fluid Prandtl number increases, due to the turbulent transport within near-wall fluid layers indicative of the largest anisotropy promoting azimuthal uniformity. However, azimuthal diffusion in near-wall regions showed to be of little importance for gaseous flow. Zeitoun [37] conducted a numerical investigation on fully developed laminar convective heat transfer in a partially heated pipe. The results revealed that the Nusselt number decreased as the angle of the heated portion of the tube surface increased, and it finally approached the Nusselt number value for a uniformly heated tube, as one might anticipate. Shen et al. [38] experimentally investigated convective heat transfer of molten salt flow with Reynolds numbers ranging from 10,000 to 67,000 and Prandtl numbers ranging from 4.5 to 8 in a circular tube under NUHF. The results showed that, under the above-mentioned conditions, the average Nusselt number is minimally influenced by heat flux non-uniformity. Okafor [39] conducted a numerical study on the influence of azimuthally NUHF on the heat transfer of an absorber tube with a thermal conductivity of 16.27 W/mK, adopting the $k-\varepsilon$ model to analyze turbulent flow with a Reynolds number ranging from 4,000 to 210,000, and employing a physical model in which the absorber tube is azimuthally divided into 36 segments for heat flux non-uniformity simulation. The results indicated that the average internal heat transfer coefficient, under the above-mentioned conditions, was not affected by heat flux non-uniformity. Zeitoun [40] numerically investigated fully developed laminar forced convective heat transfer in a partially heated tube. The results revealed how the Nusselt number decreases with the increase in peripheral heating angle and increases with the increase in tube wall thickness. Okafor et al. [41] investigated the influence of NUHF on convective heat transfer in a tube with secondary buoyancy-driven laminar flow. It was found that the average internal heat transfer coefficient increased with the NUHF intensity, the incident heat flux angle span, and the inlet fluid temperature. Huang et al. [42] performed a numerical study on combined natural and forced convection in the fully developed turbulent region

of a non-uniformly heated horizontal tube for a Reynolds number range from 2×10^4 to 10^5, Prandtl number of 1.5, and Grashof number ranging from 0 to 10^{12}. The results showed that the Nusselt number of turbulent mixed convection for non-uniformly heated tubes was larger than that for uniformly heated tubes. Okafor et al. [43] numerically investigated the influence of non-uniform azimuthal heat flux on a horizontal tube with a turbulent mixed convection regime. The results showed that the internal heat transfer characteristics are affected by buoyancy-driven secondary flow for Reynolds numbers lower than 9100. However, contrary to the aforementioned studies, the results indicated that the internal heat transfer coefficients and correlations are independent of azimuthal heat transfer intensities and distributions for Reynolds numbers higher than 9100. In another study, Okafor et al. [44] launched an investigation into laminar mixed convection in a non-uniformly heated horizontal tube, for a Reynolds number range from 130 to 2000. The results showed that, due to buoyancy effects, the internal heat transfer coefficient increased as the azimuthally NUHF span increased. Seco-Nicolas et al. [45] conducted a numerical study on laminar forced-convection heat transfer within a tube with steady-state and asymmetric thermal boundary conditions. They considered axial fluid conduction and wall thickness conduction effects in their analysis, maintaining a constant external temperature on the upper side and insulating the lower side of the tube. It was found that different temperature values exist for different azimuthal angles due to the asymmetric thermal conditions. An experimental study on the convective heat transfer in a turbulent liquid metal flow through a tube with azimuthally inhomogeneous heat flux was recently performed by Laube et al. [46]. For a Peclet number range from 1400 to 3600, it was revealed that the azimuthally averaged Nusselt number was not influenced by azimuthally inhomogeneous heat flux, and thus, the correlations for azimuthally UHF could be applied to predict the case of inhomogeneous heat flux.

This study specifically focuses on investigating the forced-convection heat transfer within a PTSC absorber tube regarding its characteristic flow behavior and boundary conditions, while few of the above-mentioned studies, inter alia, have focused on the thermal behavior of the flow inside a tube exposed to azimuthally NUHF, especially a horizontal tube flow [45], as in a PTSC absorber tube. The current study employs a model to analyze the conjugate heat transfer within a PTSC absorber tube with a turbulent forced-convection heat transfer and under azimuthally NUHF.

This study aims to further elucidate the influence of azimuthally NUHF distributions on forced-convection heat transfer (Nusselt number and convective heat transfer coefficient) in a smooth horizontal tube. Additionally, the effect of tube material conductivity and thickness on the convective heat transfer is analyzed. The analysis is conducted for turbulent flow within a Reynolds number range from 10,000 to 110,000 and Prandtl number values of 7.25, 0.3566, and 15.74. This Reynolds number range corresponds to the typical turbulent regime relevant to the intended applications, such as PTSCs, as reported in relevant studies [6,16,47]. The selected Prandtl numbers are assumed to be in the same order of magnitude as those from similar research [48–50], representing thermal oils[1] commonly employed as heat transfer fluids and their possible operating temperature ranges in this study. The tube wall thickness and diameter are considered to be 3 mm and 60 mm, respectively, as in most of the abovementioned research [51–53], where tube diameters are of similar magnitude, and tube thickness

[1] Behran Oil brand is considered as the thermal oil in the current research.

are sufficiently small (up to 3.5 mm) that wall conduction resistance can be neglected. The length-to-diameter ratio for the tube is approximately 166, ensuring fully developed flow according to [36]. The tube material used for the core calculations is stainless steel 316 (AISI 316), as commonly applied in the aforementioned studies [14,52,54].

To achieve azimuthally NUHF distributions around the tube, the tube is divided into as many equal sections as computational cost allows, while ensuring the desired accuracy of results. In this study, this corresponded to eight sections. Various degrees of azimuthal non-uniformities are created by insulating some sections while heating others. The heat flux applied over the tube surface is presumed to vary from 10,000 W/m^2 (i.e., azimuthally UHF), to 80,000 W/m^2 (i.e., the most azimuthally NUHF). This range of heat flux covers several applications, including PTSCs, whose common azimuthal heat flux seldom exceeds 50,000 W/m^2 [51,53,54], depending on the local concentration ratio (LCR) distributions. The buoyancy effect is neglected since the Richardson number is very small (< 0.05), indicating only forced convection with no secondary flow emergence in the tube [55]. Equation (2) represents the general definition of the Richardson number [43].

$$\mathrm{Ri} = \frac{\mathrm{Gr}}{\mathrm{Re}^2} \tag{2}$$

where Gr and Re are the Grashof and Reynolds numbers, respectively.

The effect of various states of heat flux non-uniformities on the average Nusselt number and temperature distribution is extensively investigated in the current study. In addition, the study examines how both the tube wall material conductivity and thickness significantly influence the deviation of the average Nusselt number with azimuthally NUHF from that with azimuthally UHF. In some numerical studies, such as [56], it has been concluded that numerical results for the average Nusselt number are in good agreement with conventional correlations, such as the Dittus-Boelter equation, regardless of factors such as Reynolds number range, absorber tube material, and PTSC LCR distribution (for solar collector applications), which indicates the degree of azimuthal heat flux non-uniformity around the absorber tube. In other words, with respect to these parameters, a categorical or generalized conclusion regarding the agreement or deviation of numerically obtained Nusselt numbers from conventional correlations is no longer justified. In other words, unlike other studies, the present study thoroughly addresses the effect of the aforementioned parameters on both the deviation and agreement stated above. Finally, a Nusselt number deviation analysis focused on PTSCs is conducted to emphasize the significance of the study model and results. Taken as a whole, the current study results, obtained through a conjugate heat transfer analysis of a PTSC absorber tube, clearly show the critical importance of taking into consideration the non-uniformity of the solar heat flux around the absorber tube in relation to the above-mentioned parameters. In fact, the study results comprehensively show how the assumption of azimuthal heat flux uniformity for an absorber tube of a parabolic trough solar collector, as made by many researchers, may lead to remarkable inaccuracies.

2. Model description

2.1. Governing equations and boundary conditions

Assuming an incompressible fluid with steady-state turbulent flow and uniform inlet velocity in a circular tube with temperature-independent constant material properties, and considering the purpose of the current study, the governing equations are expressed as follows [57]:

Continuity equation: $\frac{1}{r}\frac{\partial}{\partial r}(rv_r)+\frac{1}{r}\frac{\partial}{\partial \theta}(v_\theta)+\frac{\partial}{\partial z}(v_z)=0$ (3)

r momentum equation: $(V\cdot\nabla)v_r-\frac{1}{r}v_\theta^2=-\frac{1}{\rho}\frac{\partial p}{\partial r}+g_r+\nu(\nabla^2 v_r-\frac{v_r}{r^2}-\frac{2}{r^2}\frac{\partial v_\theta}{\partial \theta})$ (4)

θ momentum equation: $(V\cdot\nabla)v_\theta+\frac{v_r v_\theta}{r}=-\frac{1}{\rho r}\frac{\partial p}{\partial \theta}+g_\theta+\nu\left(\nabla^2 v_\theta+\frac{2}{r^2}\frac{\partial v_r}{\partial \theta}-\frac{v_\theta}{r^2}\right)$ (5)

z momentum equation: $(V\cdot\nabla)v_z=-\frac{1}{\rho}\frac{\partial p}{\partial z}+g_z+\nu(\nabla^2 v_z)$ (6)

Energy equation: $\rho c_p[(V\cdot\nabla)T]=k\nabla^2 T+\mu\left[2\left(\epsilon_{rr}^2+\epsilon_{\theta\theta}^2+\epsilon_{zz}^2\right)+\epsilon_{\theta z}^2+\epsilon_{rz}^2+\epsilon_{r\theta}^2\right]$ (7)

In all above-mentioned equations [57],

$$V\cdot\nabla=v_r\frac{\partial}{\partial r}+\frac{1}{r}v_\theta\frac{\partial}{\partial \theta}+v_z\frac{\partial}{\partial z}$$

$$\nabla^2=\frac{1}{r}\frac{\partial}{\partial r}\left(r\frac{\partial}{\partial r}\right)+\frac{1}{r^2}\frac{\partial^2}{\partial \theta^2}+\frac{\partial^2}{\partial z^2}$$

$\epsilon_{rr}=\frac{\partial v_r}{\partial r}$; $\epsilon_{\theta\theta}=\frac{1}{r}\frac{\partial v_\theta}{\partial \theta}+\frac{v_r}{r}$; $\epsilon_{zz}=\frac{\partial v_z}{\partial z}$; $\epsilon_{\theta z}=\frac{1}{r}\frac{\partial v_z}{\partial \theta}+\frac{\partial v_\theta}{\partial z}$; $\epsilon_{rz}=\frac{\partial v_r}{\partial z}+\frac{\partial v_z}{\partial r}$; $\epsilon_{r\theta}=\frac{1}{r}\frac{\partial v_r}{\partial \theta}+\frac{\partial v_\theta}{\partial r}-\frac{v_\theta}{r}$

The transport equations of turbulence kinetic energy (k) and turbulence frequency (ω) can be found in [58].

In these equations, ρ is density, p is pressure, v is velocity, ν is kinematic viscosity, g is gravitational acceleration, r is the radial distance in cylindrical coordination or tube radius, z is the axial distance in cylindrical coordination, θ is the angular measure in cylindrical coordination, k is thermal conductivity, and c_p is the specific heat capacity at constant pressure.

To simulate azimuthally non-uniform boundary heat flux in the absorber tube of a PTSC, a simplified local concentration ratio distribution (LCR) is assumed. Consequently, a simplified azimuthal NUHF profile is used, with one heated span and one adiabatic span along the tube circumference, following the approach of Malekan et al. [59]. In their work, the complex NUHF profile was approximated using a simplified representation, introducing an error of less than 5%. This simplification, contrary to the assumptions in which the non-uniformity of the heat flux around the absorber tube is totally ignored, retains the validity of the NUHF assumption while ensuring a small error. This approximation clearly justifies the model employed in the current study regarding the various NUHF boundary conditions applied to the absorber tube.

Furthermore, the present model effectively describes convective heat transfer within absorber tubes of PTSCs with various LCR distributions. By considering PTSC local concentration ratio (LCR) distributions, which depend on geometric features of PTSC, such as collector aperture width, rim angle,

and absorber tube diameter, the model can analyze various azimuthally non-uniform boundary heat flux distributions [60]. For this study, the collector aperture width and absorber tube diameter are constant, while various rim angles are assumed. As studied by He et al. [61] and Agagna et al. [62], rim angles influence LCR distributions and NUHF distribution around the absorber tube. Accordingly, this study considers multiple NUHF states arising from different rim angles. Beyond solar thermal applications, this model generalizes to other industrial applications, such as heat exchangers [63]. By simulating azimuthally non-uniform boundary heat flux distributions, the model enables the analysis of various non-uniformity states, each with one heated span and one adiabatic span. This versatility highlights the model's advantages compared to others.

2.2. Numerical method

As a model capable of addressing near-wall shear stress and heat transfer, the $SST\ k-\omega$ model is employed in this study as an ideal turbulence model to analyze forced convection heat transfer and the average Nusselt number in the tube. In other words, since the accuracy in calculating near-wall parameters, such as the average Nusselt number, plays a key role in the current research, the $SST\ k-\omega$ model is preferred as a strong model capable of y^+-sensitive wall treatment [58]. The use of the $SST\ k-\omega$ turbulence model was also shown to be more suitable than other RANS models for describing tube wall heat transfer, characterized by the Nusselt number [11].

A three-dimensional CFD analysis using the finite volume method is performed in ANSYS Fluent 18.2 software to simulate the model. First, two tube geometries were designed in ANSYS DesignModeler: one with a very small thickness and negligible thermal conduction resistance, and the other with no thickness consideration. These geometries were then transferred to ANSYS ICEM CFD. Subsequently, the tube was azimuthally divided into eight equal sections, i.e., eight wall sections of 45° of the tube perimeter, to simulate non-uniformity states of azimuthal heat flux. After sectioning the tube, an O-grid treatment was performed to produce a high-quality mesh. Finally, as shown in Figure 2, grids were generated within both the fluid and the solid domains of the tube. The mesh size and quality were examined accurately by exporting the mesh quality factor, showing the minimum quality of 0.664 and the maximum quality of 0.996 out of 1, for the worst-meshed parts and the best-meshed parts, respectively. The meshed tube was then transferred to ANSYS Fluent for numerical calculations. For these simulations, the SIMPLE algorithm suggested by Patankar and Spalding [64] was applied to couple pressure and velocity. A second-order upwind scheme was used to discretize the momentum, energy, k, and ω equations. The Green-Gauss node-based method was employed to compute gradients. The convergence absolute criteria for the solution of the above-mentioned equations were all set based on a residual value of 10^{-6}, which showed good accuracy. The accuracy was verified by monitoring one thermal property, such as the tube outlet temperature, and confirming that it remained constant beyond a certain iteration. To control the update of computed variables at each iteration, the under-relaxation factors were set to 0.3 for the pressure variable, 1 for density, body forces, turbulent viscosity, and energy variables, and 0.8 for turbulent kinetic energy and specific dissipation rate.

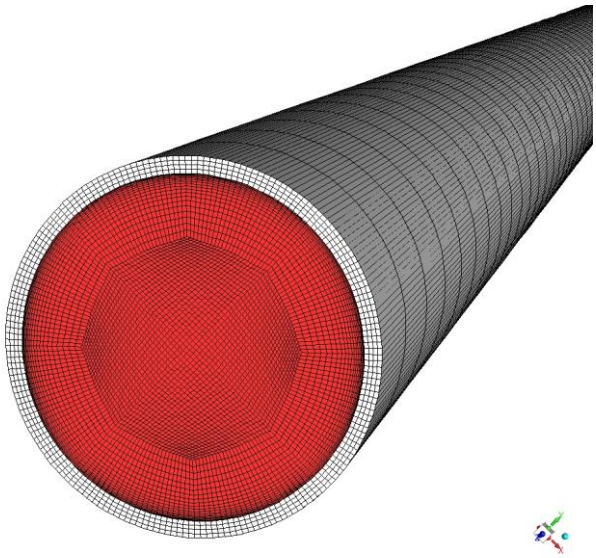

Figure 2. Partially depicted meshed solid and fluid domains of the tube, including thickness, used in the numerical solution.

2.3. Grid independency

In order to ensure the accuracy of the numerical results, grid independency tests were performed for Nusselt number of Re = 10,000, Re = 60,000, and Re = 110,000, with an azimuthal UHF of $q'' = 10{,}000$ W/m^2 As presented in Table 1 to 3, grid independencies were achieved for the Nusselt number at Re = 10,000, Re = 60,000, and Re = 110,000 after three, two, and four program runs, respectively. The results yielded Nu = 63.515 with a total node count of 2,726,800, Nu = 345.069 with a total node count of 1,562,700, and Nu = 583.898 with a total node count of 3,548,896, respectively. The grid independency tests showed a Nusselt number value difference percentage on the order of 10^{-2} or 10^{-3}, which is satisfactorily small.

Table 1. Grid independency test results for the Nusselt number at Re = 10,000.

Total number of nodes	Nu	$\left\|\frac{Nu_{i+1} - Nu_i}{Nu_{i+1}}\right\| \times 100$
851,400	63.116	-
1,562,700	63.513	0.625
2,726,800	63.515	0.003

Table 2. Grid independency test results for the Nusselt number at Re = 60,000.

Total number of nodes	Nu	$\left\|\frac{Nu_{i+1} - Nu_i}{Nu_{i+1}}\right\| \times 100$
851,400	345.030	-
1,562,700	345.069	0.01

Table 3. Grid independency test results for the Nusselt number at Re = 110,000.

Total number of nodes	Nu	$\left\|\frac{Nu_{i+1}-Nu_i}{Nu_{i+1}}\right\| \times 100$
851,400	586.335	-
1,562,700	584.544	0.30
2,726,800	583.563	0.16
3,548,896	583.898	0.05

2.4. Code validation

To validate the numerical CFD results of the present study, the numerical results obtained for the average Nusselt number with azimuthally UHF are compared with the Dittus-Boelter and Gnielinski correlations. The Dittus-Boelter and Gnielinski equations are expressed as follows, respectively [17]:

$$Nu = 0.023 Re^{0.8} Pr^{0.4} \tag{8}$$

$$Nu = \frac{\left(f/8\right)(Re_D - 1000)Pr}{1 + 12.7\left(f/8\right)^{1/2}\left(Pr^{2/3} - 1\right)} \tag{9}$$

where f is the friction factor and is calculated using the Petukhov correlation [17]:

$$f = (0.790\, ln\, Re_D - 1.64)^{-2} \tag{10}$$

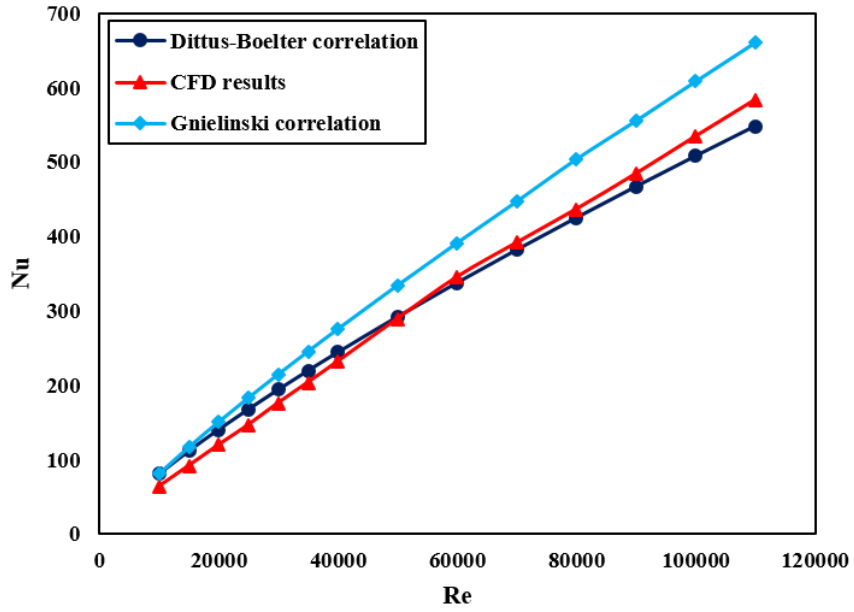

Figure 3. Validation and comparison of CFD Nusselt number values with the Dittus-Boelter and Gnielinski equations vs. Reynolds number, regarding a uniform heat flux.

All the numerical results obtained for the average Nusselt number with UHF at various Reynolds numbers, along with the corresponding Nusselt number values from the Dittus-Boelter and Gnielinski equations, at Pr = 7.25, are depicted in Figure 3. As observed, the numerical results at certain Reynolds numbers are in nearly complete agreement with the Dittus-Boelter equation and, to some extent, with the Gnielinski equation. However, the numerical results for the Nusselt number show better agreement with the Dittus-Boelter equation than with the Gnielinski equation. On average, there is a Nusselt number deviation error of approximately 7% from the Dittus-Boelter equation across the entire Reynolds number range. This deviation indicates satisfactorily accurate CFD results regarding the maximum possible errors of 25% and 10% that may arise from using the Dittus-Boelter and Gnielinski equations, respectively [17].

3. Results and discussion

3.1. Average Nusselt number for Pr = 7.25

Regarding the equal tube wall sections of 45° mentioned above, Table 4 presents seven heat flux non-uniformity states in addition to one UHF state for the tube. The total heat transfer rate received by the tube is assumed to remain constant for all states, as per the study assumptions. For instance, in the 135°-insulated state, an azimuthal heat flux of 16,000 W/m^2 is applied to the 225°-heated span, while a flux of 10,000 W/m^2 is assumed for the UHF state, ensuring the total heat transfer rate remains constant across all seven aforementioned states.

Table 4. Insulated and heated tube spans, regarding heat flux distributions onto the heated spans, with a constant total heat transfer onto the tube.

Insulated span angle, θ (°)	0°	45°	90°	135°	180°	225°	270°	315°
Heated span angle (°)	360° (UHF)	315°	270°	225°	180°	135°	90°	45°
Heat flux, q'' (W/m^2)	10,000	11,428.57	13,333.33	16,000	20,000	26,666.66	40,000	80,000

Figure 4 illustrates the Nusselt number variation against the Reynolds number for all previously mentioned heat flux non-uniformity states, as well as the heat flux uniformity state. As shown in Figure 4, the Nusselt number values in NUHF states are consistently lower than that in the UHF state. Furthermore, it is observed that the Nusselt number in NUHF states decreases as the insulation span angle increases. For instance, the Nusselt number deviation at the Reynolds number value of 50,000, for various insulation angles of 45°, 135°, 225°, and 315°, is 3%, 13%, 26.34%, and 39.56%, respectively. It should be noted that the insulation span and the heating span in each NUHF state are independent of their location on the tube circumference, as the buoyancy effect is negligible. Figure 4 also shows that the deviation of the Nusselt number in NUHF states from that in the UHF state is more remarkable in higher Reynolds number values. This decrease in the Nusselt number values at higher Reynolds numbers is due to the varying temperature gradient. As a case in point, the Nusselt number deviation at the insulation angle of 135°, at various Reynolds number values of 10,000, 35,000, 50,000, and 110,000, is 3.5%, 9.2%, 13%, and 15.5%, respectively. Additionally, it should be mentioned that these Nusselt number reductions, due to the heat flux non-uniformities, may remarkably influence the

collector's performance. In other words, as mentioned by Jamali [65], the reduction in the Nusselt number value will result in a decrease in PTSC thermal efficiency, and consequently, a decrease in the collector performance. Figure 5 provides a schematic cross-sectional representation of the azimuthal insulation angle (θ) around the tube.

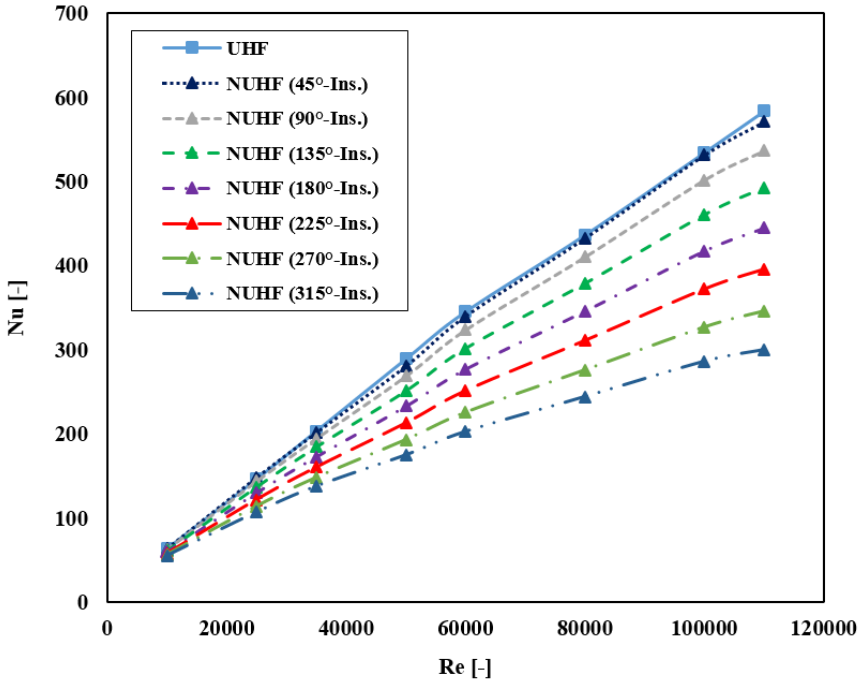

Figure 4. Comparison of CFD Nusselt number values under uniform heat flux and various non-uniform states versus Reynolds number for a tube made of AISI 316 (Pr = 7.25).

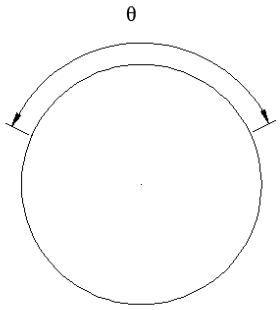

Figure 5. Schematic view of a tube cross-section with insulation angle span.

A new general correlation for the Nusselt number was developed, applicable for both UHF and NUHF states under the current study conditions. The Nusselt number correlation obtained is as follows:

$$Nu_{NUHF} = Nu_{UHF} - B \times Re^{\alpha} \qquad @Pr = 7.25 \tag{11}$$

where B coefficient and α exponent correlations were both obtained as functions of the insulation span angle (θ). Both B and α are thermal parameters, which depend on the azimuthal heat flux non-uniformity. These were derived by plotting a power regression trendline and a polynomial trendline, respectively, using the least squares method, which yielded a high R-squared value of more than 0.99, as depicted in Figure 6. This high R-squared value indicates the high precision of the correlations. The formulations obtained are as follows:

$$B(\theta) = 7 \times 10^{-13} \times \theta^{2.9417} \tag{12}$$

$$\alpha(\theta) = (4 \times 10^{-6})\theta^2 - 0.0022\theta + 1.7602 \tag{13}$$

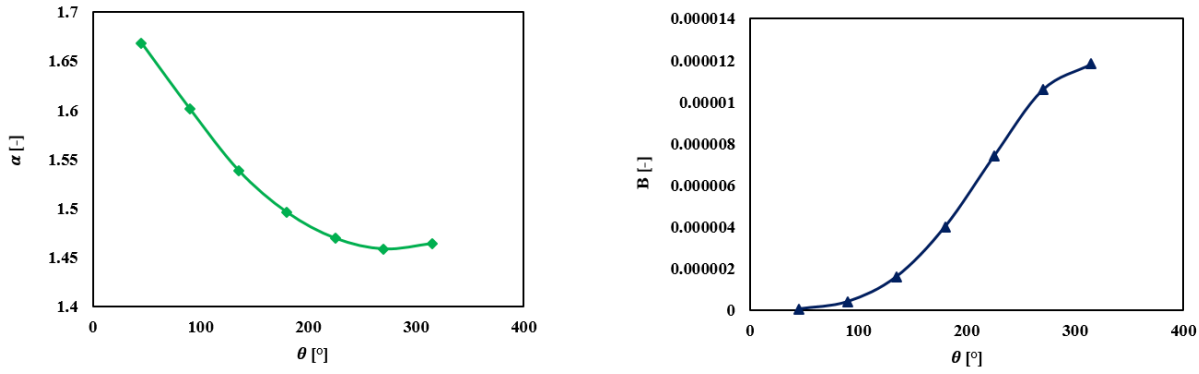

(a) (b)

Figure 6. (a) Exponent and (b) Coefficient of the Nusselt number correlation, as functions of insulation span angle.

Equation (11) clearly illustrates the trend of the Nusselt number deviation under NUHF conditions relative to that under uniform heat flux, as a function of the tube's insulation span angle.

3.2. The effect of the Prandtl number

In section 3.1, the Nusselt number deviation under various degrees of heat flux non-uniformity and different Reynolds numbers, relative to the Nusselt number under UHF, was comprehensively discussed for a Prandtl number of 7.25. In this section, a concise discussion is provided for two other Prandtl numbers, i.e., 0.3566 and 15.74. Figures 7 and 8 demonstrate the Nusselt number deviation at various degrees of heat flux non-uniformity and Reynolds numbers for Prandtl numbers of 0.3566 and 15.74, respectively. Figures 7 and 8, along with Figure 4, clearly illustrate that higher deviations of the Nusselt number are observed at higher Prandtl number values. As a matter of fact, the average Nusselt number is more sensitive to the heat flux non-uniformity degree under higher Prandtl numbers than in lower ones. In other words, the average Nusselt number is more sensitive to the degree of heat flux non-uniformity at higher Prandtl numbers than at lower ones. When momentum transfer dominates over heat transfer within the fluid, the effect of this non-uniformity on the deviation of the

average Nusselt number under NUHF state from that in UHF state is more significant. Consequently, at higher Prandtl numbers, the assumption of azimuthal heat flux uniformity on an absorber tube of a PTSC may lead to inaccurate results.

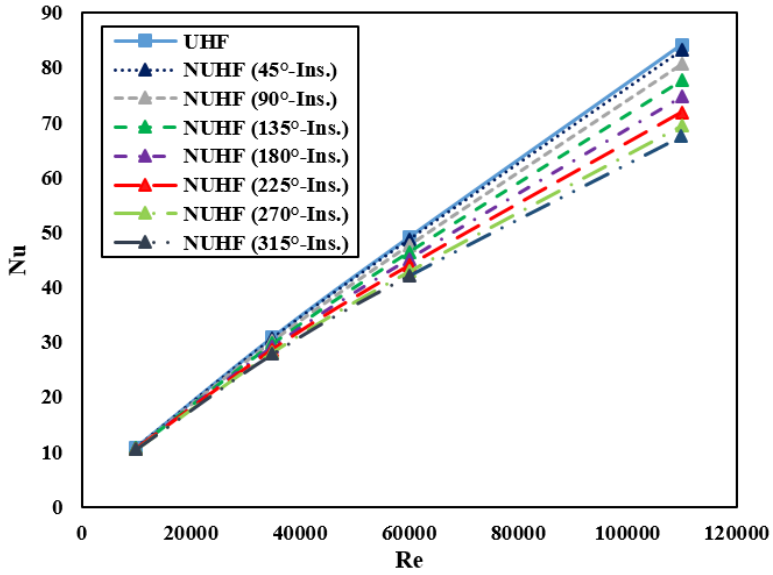

Figure 7. Comparison of CFD Nusselt number values under uniform heat flux and various non-uniform states versus Reynolds number for a tube made of AISI 316 (Pr = 0.3566).

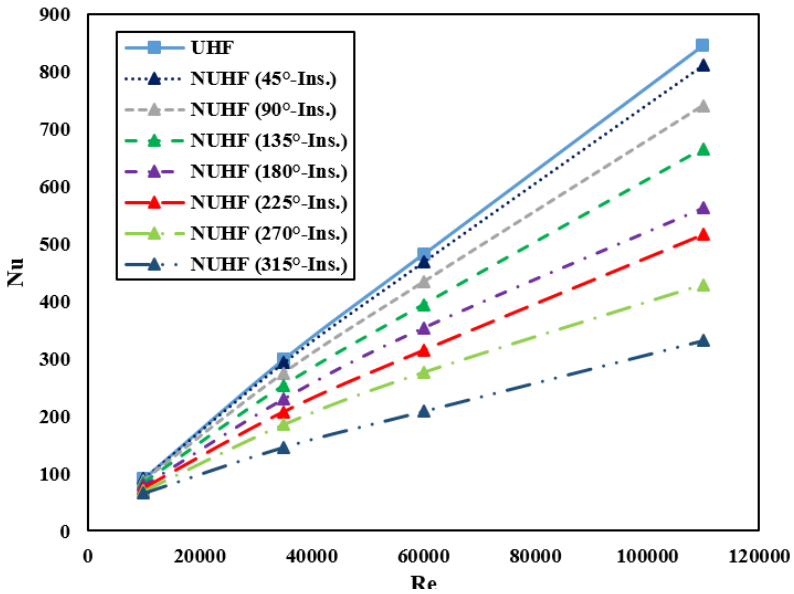

Figure 8. Comparison of CFD Nusselt number values under uniform heat flux and various non-uniformity states versus Reynolds number for a tube made of AISI 316 (Pr = 15.74).

3.3. The effect of tube material conductivity and thickness

Almanza et al. [66] conducted experimental research into the effects of tube thermal conductivity on the temperature difference within tube walls, heat transfer, and mechanical problems. Flores et al. [67] presented a bimetallic absorber tube (copper-steel) that improves heat transfer and minimizes mechanical problems. In another study, they employed another bimetallic absorber tube (Cu-Fe) under transient conditions and stratified two-phase flow, with the purpose of mitigating mechanical problems. Wang et al. [68] performed a numerical analysis of receiver tubes made of various materials (aluminum, copper, silicon carbide, and stainless steel), showing how thermal conductivity significantly reduces the mechanical stress failure in the tube.

In the current study, as Figure 9 clearly reveals, the tube material conductivity and thickness significantly influence the average Nusselt number with azimuthally NUHF. Figure 9 presents the variation of the Nusselt number with Reynolds number for the most azimuthally NUHF distribution (315° insulated), considering five tube materials: pure aluminum (k = 237 W/mK), pure nickel (k = 90.7 W/mK), carbon steel AISI 1010 (k = 63.9 W/mK), stainless steel AISI 316 (k = 17.5 W/mK), and Nichrome (k = 12 W/mK), in along with a tube without thickness.

The results show that pure aluminum with higher thermal conductivity exhibits only a small deviation between the Nusselt number with azimuthally NUHF and that with azimuthally UHF. For Nichrome, having lower thermal conductivity, there is a large deviation between the Nusselt number with azimuthally NUHF and that with azimuthally UHF. It is also observed that deviations are smaller at lower Reynolds numbers and increase with Reynolds number, as in the case of the aluminum tube, where the deviation at lower Reynolds numbers is negligible due to its very high conductivity. Hence, the Nusselt number deviation is more pronounced for materials with lower conductivity and at higher Reynolds numbers. The negligible deviation in lower Reynolds numbers for pure aluminum indicates near-complete agreement between the NUHF and UHF Nusselt numbers. However, there is no such agreement observed for very-low-conductivity materials, such as Nichrome alloy, even at lower Reynolds number values. In other words, small Nusselt number deviations in high-conductivity tubes and large Nusselt number deviations in very-low-conductivity tubes reflect the very low and very high temperature gradient variations within these materials, respectively. It should also be mentioned that other factors related to tube material may influence heat-flux uniformity, but these fall outside of the scope of this research. For example, the application of high-conductivity coatings is worth further research, as evaluated by Jamali [69], although focused only on PTSC radiation heat transfer.

Additionally, for the tube with no thickness consideration, the Nusselt number deviation from that with UHF is the largest among all configurations, regardless of thermal conductivity. As a case in point, for a fluid with Pr = 7.25 and Re = 60,000 in a 315°-insulated tube, the average Nusselt number deviation values for the tube materials of Al, Ni, AISI 1010, AISI 316, Nichrome, and no-thickness tube are 2.8%, 12.35%, 16.8%, 40%, 45.9%, and 84.7%, respectively.

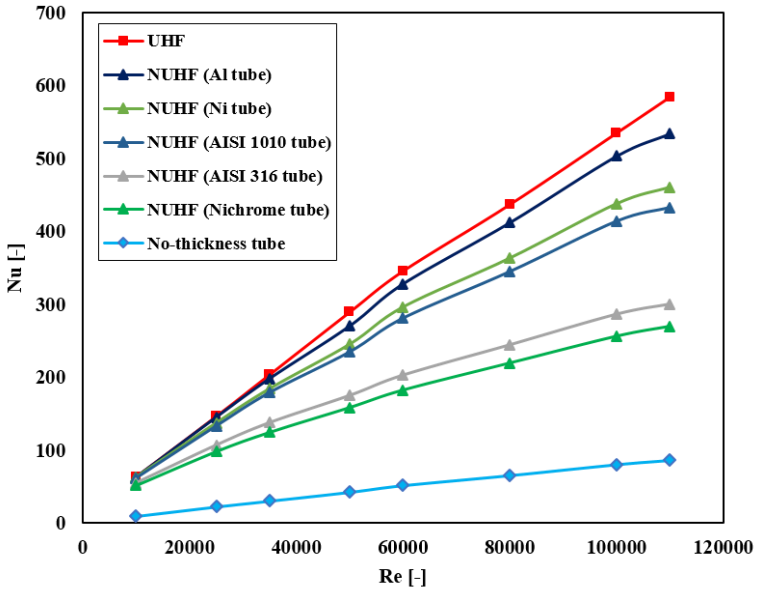

Figure 9. The effect of tube material conductivity and thickness on the deviation of the Nusselt number with non-uniform heat flux (for the 315°-insulated tube) from the Nusselt number with uniform heat flux vs. Reynolds number (Pr = 7.25).

3.4. Nusselt number deviation analysis

In this section, the Nusselt number deviation under NUHF conditions, relative to the UHF condition, is analyzed with respect to the application of the current study results, with an emphasis on PTSCs, to better elucidate the importance of the results. As mentioned earlier, several studies have already been conducted on PTSCs' thermal efficiency and have assumed a UHF around collector absorber tubes for simplicity, despite the fact that the azimuthal heat flux is non-uniform in reality. Consequently, the analytically predicted thermal efficiencies may contain considerable errors, especially when the assumption of flux uniformity does not hold, such as in absorber tubes with large surface regions with no reflected solar irradiation from the PTSC mirror. The present results and technical procedure comprehensively address this issue, demonstrating that a Nusselt number deviation caused by assuming heat-flux uniformity is significant, depending on the degree of heat flux non-uniformity and the Reynolds and Prandtl numbers.

For this analysis, an absorber tube made of AISI 316 material is assumed. All other specifications of the absorber tube and the heat transfer fluid are assumed to be exactly the same as those in the main study. To investigate average Nusselt number deviation, the problem is examined at various Reynolds and Prandtl numbers and degrees of heat flux non-uniformity. Eqs (14) and (15) represent the general definitions for the Prandtl and Reynolds numbers, respectively [17].

$$\mathrm{Pr} = \frac{\nu}{\alpha} \tag{14}$$

$$\mathrm{Re} = \frac{\rho u D_i}{\mu} \tag{15}$$

where D_i is the tube internal diameter, ν is kinematic viscosity, α is thermal diffusivity, ρ is density, u is flow velocity, and μ is dynamic viscosity.

As stated in section 2.1, an infinite number of LCR distributions, and thus, azimuthally NUHF distributions onto an absorber tube, may exist regarding the geometric features of PTSC. Hence, the insulation span angle (θ) directly depends on the LCR distribution. In terms of solar thermal applications, this study assumes that the LCR distribution consists of one heated span and one insulated span, following Malekan et al. [59], who showed that this simplification captures NUHF effects with minimal error. In terms of PTSC design, a reduction in the collector rim angle may affect the LCR distribution [62] and result in a relatively more uniform heat flux, lower Nusselt number deviation, and, consequently, better collector performance.

For the current analysis, the Nusselt number deviation is first calculated at various insulation span angles and Reynolds numbers at a Prandtl number of 7.25, using Eq (11). Then, the effect of the Prandtl number on the Nusselt number deviation for various Reynolds numbers and at a very high degree of non-uniformity (i.e., insulation span angle of 315°) is analyzed. Figure 10 illustrates the effect of the Reynolds number and heat flux non-uniformity degree on the Nusselt number deviation. It is clearly observed that the average Nusselt number deviation increases as the heat flux non-uniformity degree increases. In each NUHF state, the Nusselt number deviation increases as the Reynolds number increases. Figure 11 shows that the higher the Prandtl number, the higher the Nusselt number deviation. Moreover, it is noteworthy that the Nusselt number deviation increases with a higher gradient in lower Reynolds number values (i.e., up to about Re = 40,000) than in higher ones. The results also indicate that the Nusselt number deviation can exceed 60% in highly NUHF distributions and high Reynolds and Prandtl numbers for an AISI 316 tube. It should be noted that the results presented in Figure 10 were obtained for a tube made of AISI 316; hence, much higher Nusselt number deviations can occur for tube materials with lower thermal conductivity than AISI 316, as observed in Figure 9. Moreover, as found in the present results and discussed in the literature review, flow regime (laminar or turbulent) and convective heat transfer type (free, forced, or mixed) both play a critical, direct role in determining the Nusselt number deviation. The Reynolds number and Richardson number indicate flow regime and convective heat transfer type, respectively; therefore, the thermal properties of the fluid indirectly affect the Nusselt number deviation. For instance, regarding flow regime, Zeitoun [37] studied laminar flow in a tube with azimuthally NUHF and reported that the Nusselt number decreased as the angle of the heated portion of the tube circumference increased. The reverse trend was observed for turbulent flow in the current study. In terms of convective heat transfer, Schmidt and Sparrow [34] examined turbulent water flow in a horizontal tube with azimuthally NUHF and found that buoyancy-affected flows tended to resist the effect of azimuthally NUHF and strengthen azimuthal uniformity due to a secondary flow presence. In contrast, buoyancy effects are negligible in the current study and therefore do not influence the results.

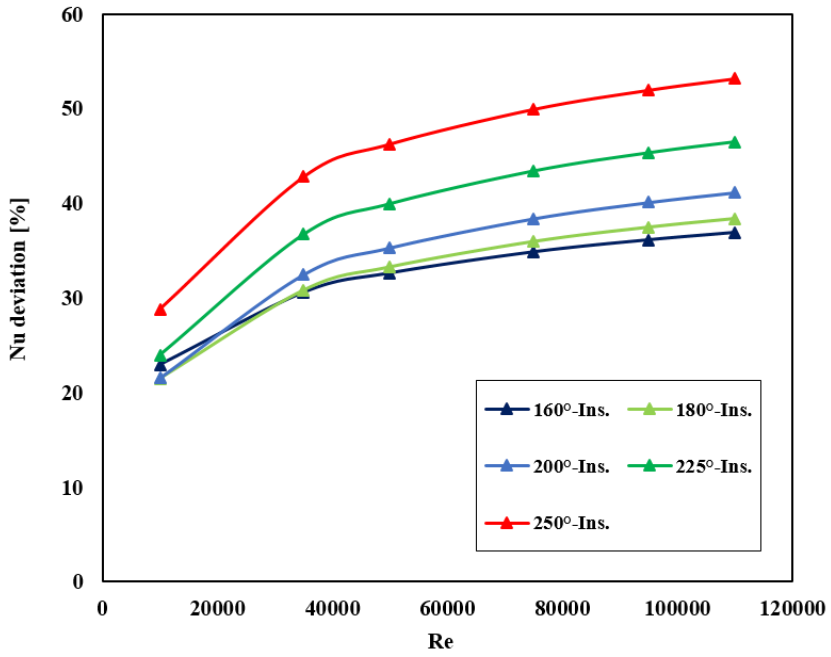

Figure 10. The Nusselt number deviation percentage at various non-uniform heat flux states in comparison with the uniform heat flux state for an AISI 316 tube (Pr = 7.25).

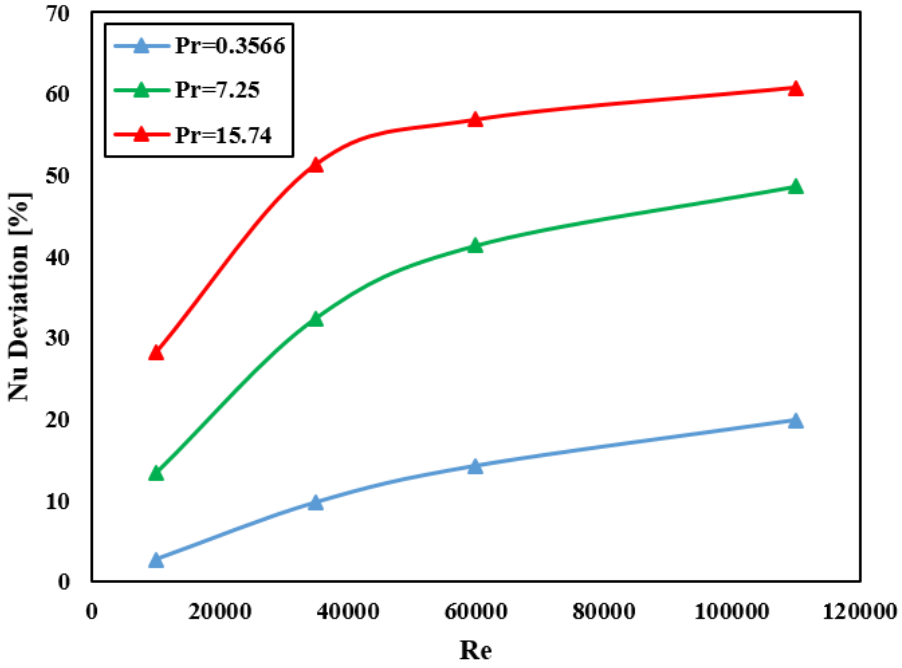

Figure 11. The Nusselt number deviation at various Prandtl and Reynolds number for an AISI 316 tube (θ = 315°).

4. Conclusions

A conjugate heat transfer analysis of a PTSC absorber tube is conducted in the current study to demonstrate how azimuthally non-uniform heat flux influences turbulent convective heat transfer in the tube. Considering a forced convection and buoyancy-unaffected heat transfer analysis in a tube with turbulent flow, the average Nusselt number with an azimuthally NUHF distribution can significantly deviate from that with azimuthally UHF. Hence, contrary to what is observed in various research works, in which conventional Nusselt number correlations, such as the Dittus-Boelter correlation, are applied for calculation simplification in spite of NUHF presence, the current research concludes that such correlations, while valid for UHF distributions, are not always appropriate in NUHF distributions. In higher Reynolds and Prandtl numbers, the aforementioned Nusselt number deviation is more significant than in lower Reynolds numbers. Moreover, higher non-uniformity degrees of the azimuthal heat flux distribution result in higher deviations of the average Nusselt number with NUHF than with UHF. The model presented in this research can be generalized to a wide variety of thermal applications with various azimuthally NUHF distributions, such as heat exchangers with smooth horizontal tubes. It should be noted, however, that such generalization is made considering the model assumptions, such as the specific ranges of the Reynolds and Prandtl numbers.

The higher the thermal conductivity of the tube material, the smaller the resulting Nusselt number deviation. For materials with very high thermal conductivity, such as pure aluminum, this conductivity effect leads to nearly complete agreement between NUHF and UHF average Nusselt numbers at lower Reynolds number values. However, this agreement is no longer observed at higher Reynolds numbers. Conversely, for tube materials with very low thermal conductivity, the influence of thermal conductivity on the Nusselt number deviation is so pronounced that no agreement between the NUHF and UHF average Nusselt numbers occurs, even at lower Reynolds numbers. The Nusselt number deviation for a tube with no thickness consideration is significantly higher than that for a tube with thickness and material conductivity effects, regardless of how low the material conductivity may be. Hence, tube thickness and material conductivity, Reynolds and Prandtl numbers, and the non-uniformity degree of azimuthal heat flux distribution around the tube, here represented by the insulation span angle (θ), may all strongly influence the Nusselt number deviation across a wide variety of applications, particularly in PTSC convective heat transfer and performance. Deviations exceeding 45% with thickness effect consideration, and over 84% without thickness, may arise from the simplifying assumption of UHF instead of NUHF boundary conditions. These findings are critical for advancing PTSC models and preventing the problems caused by azimuthally non-uniform solar heat flux, which can lead to spurious results and lower collector performance due to the NUHF boundary condition.

Prospective work: Regarding the effect of tube thickness consideration on the average Nusselt number, an analysis of conjugate heat transfer can be conducted with respect to various tube thicknesses and consequent thermal conduction resistance values. Additionally, high-conductivity tube coating applications can be studied. Other factors, such as the effect of the transient state, can also be taken into account.

Use of AI tools declaration

The author declares he has not used Artificial Intelligence (AI) tools in the creation of this article.

Acknowledgement

The author would like to appreciate the helpful guidelines issued by Dr. Amir Omidvar and Dr. Reza Mehryar.

Conflicts of interest

The authors declare no conflicts of interest.

References

1. Jamali H (2019) Investigation and review of mirrors reflectance in parabolic trough solar collectors (PTSCs). *Energy Rep* 5: 145–158. https://doi.org/10.1016/j.egyr.2019.01.006
2. Hadi Attia ME, Abdel-Aziz MM, Khelifa A (2025) A numerical approach to enhance the performance of double-pass solar collectors with finned photovoltaic/thermal integration. *Appl Therm Eng* 268: 125974. https://doi.org/10.1016/j.applthermaleng.2025.125974
3. Cheng ZD, He YL, Cui FQ, et al. (2012) Numerical simulation of a parabolic trough solar collector with nonuniform solar flux conditions by coupling FVM and MCRT method. *Sol Energy* 86: 1770–1784. https://doi.org/10.1016/j.solener.2012.02.039
4. Cheng ZD, He YL, Qiu Y (2015) A detailed nonuniform thermal model of a parabolic trough solar receiver with two halves and two inactive ends. *Renewable Energy* 74: 139–147. https://doi.org/10.1016/j.renene.2014.07.060
5. Bellos E, Tzivanidis CN, Antonopoulos KA, et al. (2016) Thermal enhancement of solar parabolic trough collectors by using nanofluids and converging—diverging absorber tube. *Renewable Energy* 94: 213–222. https://doi.org/10.1016/j.renene.2016.03.062
6. Bellos E, Tzivanidis CN (2017) Parametric analysis and optimization of an Organic Rankine Cycle with nanofluid based solar parabolic trough collectors. *Renewable Energy* 114: 1376–1393. https://doi.org/10.1016/j.renene.2017.06.055
7. Dirker J, Meyer JP, Reid W (2018) Experimental investigation of circumferentially non-uniform heat flux on the heat transfer coefficient in a smooth horizontal tube with buoyancy driven secondary flow. *Exp Therm Fluid Sci* 98: 480–496. https://doi.org/10.1016/j.expthermflusci.2018.06.017
8. Bellos E, Tzivanidis C (2018) Analytical expression of parabolic trough solar collector performance. *Designs* 2: 9. https://doi.org/10.3390/designs2010009
9. Bellos E, Tzivanidis C, Said Z (2020) A systematic parametric thermal analysis of nanofluid-based parabolic trough solar collectors. *Sustainable Energy Technol Assess* 39: 100714. https://doi.org/10.1016/j.seta.2020.100714

10. Lu J, Ding J, Yang J, et al. (2013) Nonuniform heat transfer model and performance of parabolic trough solar receiver. *Energy* 59: 666–675. https://doi.org/10.1016/j.energy.2013.07.052
11. Faheem A, Ranzi G, Fiorito F, et al. (2016) A numerical study of turbulent mixed convection in a smooth horizontal pipe. *J Heat Transfer* 138: 012501. https://doi.org/10.1115/1.4031112
12. Hachicha AA, Rodríguez I, Capdevila R, et al. (2013) Heat transfer analysis and numerical simulation of a parabolic trough solar collector. *Appl Energy* 111: 581–592. https://doi.org/10.1016/j.apenergy.2013.04.067
13. Wang Y, Liu Q, Lei J, et al. (2014) A three-dimensional simulation of a parabolic trough solar collector system using molten salt as heat transfer fluid. *Appl Therm Eng* 70: 462–476. https://doi.org/10.1016/j.applthermaleng.2014.05.051
14. Bellos E, Tzivanidis C, Tsimpoukis D (2018) Thermal, hydraulic and exergetic evaluation of a parabolic trough collector operating with thermal oil and molten salt based nanofluids. *Energy Convers Manage* 156: 388–402. https://doi.org/10.1016/j.enconman.2017.11.051
15. Marefati M, Mehrpooya M, Shafii MB (2018) Optical and thermal analysis of a parabolic trough solar collector for production of thermal energy in different climates in Iran with comparison between the conventional nanofluids. *J Cleaner Prod* 175: 294–313. https://doi.org/10.1016/j.jclepro.2017.12.080
16. Quezada-García S, Sánchez-Mora H, Polo-Labarrios MA, et al. (2019) Modeling and simulation to determine the thermal efficiency of a parabolic solar trough collector system. *Case Stud Therm Eng* 16: 100523. https://doi.org/10.1016/j.csite.2019.100523
17. Bergman TL, Lavine AS, Incropera FP, et al. (2011) Fundamentals of heat and mass transfer (7th ed.). Wiley. Available from: https://bcs.wiley.com/he-bcs/Books?action=index&itemId=0470501979&bcsId=6563.
18. Norouzi AM, Siavashi M, Ahmadi R, et al. (2021) Experimental study of a parabolic trough solar collector with rotating absorber tube. *Renewable Energy* 168: 734–749. https://doi.org/10.1016/j.renene.2020.12.088
19. Norouzi AM, Siavashi M, Oskouei MK (2020) Efficiency enhancement of the parabolic trough solar collector using the rotating absorber tube and nanoparticles. *Renewable Energy* 145: 569–584. https://doi.org/10.1016/j.renene.2019.06.027
20. Bezaatpour M, Rostamzadeh H, Bezaatpour J (2021) Hybridization of rotary absorber tube and magnetic field inducer with nanofluid for performance enhancement of parabolic trough solar collector. *J Cleaner Prod* 283: 124565. https://doi.org/10.1016/j.jclepro.2020.124565
21. Khanna S, Singh S, Kedare SB (2015) Explicit expressions for temperature distribution and deflection in absorber tube of solar parabolic trough concentrator. *Sol Energy* 114: 289–302. https://doi.org/10.1016/j.solener.2015.01.044
22. Adebiyi GA, Hall W (1976) Experimental investigation of heat transfer to supercritical pressure carbon dioxide in a horizontal pipe. *Int J Heat Mass Transfer* 19: 715–720. https://doi.org/10.1016/0017-9310(76)90123-X
23. Ghajar AJ, Tam LM (1994) Heat transfer measurements and correlations in the transition region for a circular tube with three different inlet configurations. *Exp Therm Fluid Sci* 8: 79–90. https://doi.org/10.1016/0894-1777(94)90075-2

24. Gnielinski V (1976) New equations for heat and mass transfer in turbulent pipe and channel flow. *Int Chem En* 16: 359–368.
25. Churchill SW (1977) Comprehensive correlating equations for heat, mass and momentum transfer in fully developed flow in smooth tubes. *Ind Eng Chem Fundam* 16: 109–116. https://doi.org/10.1021/i160061a021
26. Boufendi T, Afrid M (2004) The physical aspect of three-dimensional mixed convection in a uniformly heated horizontal pipe. *Sci Technol*, 39–52. Available from: https://www.academia.edu/98296662/The_Physical_Aspect_of_Three_Dimensional_Mixed_Convection_in_a_Uniformly_Heated_Horizontal_Pipe.
27. Mohammed HA, Salman YK (2007) Experimental investigation of mixed convection heat transfer for thermally developing flow in a horizontal circular cylinder. *Appl Therm Eng* 27: 1522–1533. https://doi.org/10.1016/j.applthermaleng.2006.09.023
28. Grassi W, Testi D (2006) Heat transfer correlations for turbulent mixed convection in the entrance region of a uniformly heated horizontal tube. *J Heat Transfer* 128: 1103–1107. https://doi.org/10.1115/1.2345436
29. Mohammed HA, Salman YK (2007) The effects of different entrance sections lengths and heating on free and forced convective heat transfer inside a horizontal circular tube. *Int Commun Heat Mass Transfer* 34: 769–784. https://doi.org/10.1016/j.icheatmasstransfer.2007.03.005
30. Testi D (2013) A novel correlation for azimuthal and longitudinal distributions of heat transfer coefficients in developing horizontal pipe flow under transitional mixed convection. *Int J Heat Mass Transfe* 60: 221–229. https://doi.org/10.1016/j.ijheatmasstransfer.2013.01.003
31. Chae MS, Chung BJ (2014) Laminar mixed-convection experiments in horizontal pipes and derivation of a semi-empirical buoyancy coefficient. *Int J Therm Sci* 84: 335–346. https://doi.org/10.1016/j.ijthermalsci.2014.06.007
32. Reynolds WC (1963) Turbulent heat transfer in a circular tube with variable circumferential heat flux. *Inter J Heat Mass Transfer* 6: 445–454. https://doi.org/10.1016/0017-9310(63)90119-4
33. Black A, Sparrow EM (1967) Experiments on turbulent heat transfer in a tube with circumferentially varying thermal boundary conditions. *J Heat Transfer* 89: 258–268. https://doi.org/10.1115/1.3614375
34. Schmidt RR, Sparrow EM (1978) Turbulent flow of water in a tube with circumferentially nonuniform heating, with or without buoyancy. *J Heat Transfer* 100: 403–409. https://doi.org/10.1115/1.3450822
35. Knowles GR, Sparrow EM (1979) Local and average heat transfer characteristics for turbulent airflow in an asymmetrically heated tube. *J Heat Transfer* 101: 635–641. https://doi.org/10.1115/1.3451049
36. Chieng CC, Launder BE (2007) On the calculation of turbulent transport in flow through an asymmetrically heated pipe. *Numer Heat Transfer* 2: 359–371. https://doi.org/10.1080/10407787908913419
37. Zeitoun O (2002) Heat transfer for laminar flow in partially heated tubes. *Alexandria Eng J* 41: 205–212. Available from: https://www.researchgate.net/publication/255618364.

38. Shen X, Lu J, Ding J, et al. (2014) Convective heat transfer of molten salt in circular tube with nonuniform heat flux. *Exp Therm fluid Sci* 55: 6–11. https://doi.org/10.1016/j.expthermflusci.2014.02.015
39. Okafor IF, Dirker J, Meyer JP (2014) Influence of circumferential solar heat flux distribution on the heat transfer coefficients of linear Fresnel collector absorber tubes. *Sol Energy* 107: 381–397. https://doi.org/10.1016/j.solener.2014.05.011
40. Zeitoun O, Conjugate Laminar forced convection in partially heated tubes. Available from: https://www.researchgate.net/publication/267948343.
41. Okafor IF, Dirker J, Meyer JP (2017) Influence of non-uniform heat flux distributions on the secondary flow, convective heat transfer and friction factors for a parabolic trough solar collector type absorber tube. *Renewable Energy* 108: 287–302. https://doi.org/10.1016/j.renene.2017.02.053
42. Huang Z, Li ZY, Tao WQ (2017) Numerical study on combined natural and forced convection in the fully-developed turbulent region for a horizontal circular tube heated by non-uniform heat flux. *Appl Energy* 185: 2194–2208. https://doi.org/10.1016/j.apenergy.2015.11.066
43. Okafor IF, Dirker J, Meyer JP (2016) Turbulent mixed convection heat transfer for non-uniform heat flux distributions on a horizontal circular tube. *Proceedings of the 12th International Conference on Heat Transfer, Fluid Mechanics and Thermodynamics (HEFAT 2016)*, 993–998. Available from: https://www.researchgate.net/publication/305496420.
44. Okafor IF, Dirker J, Meyer JP (2019) Asymmetrical non-uniform heat flux distributions for laminar flow heat transfer with mixed convection in a horizontal circular tube. *Heat Transfer Eng* 40: 109–127. https://doi.org/10.1080/01457632.2017.1421055
45. Seco-Nicolás M, Alarcón M, Luna-Abad JP (2021) 3D numerical simulation of laminar forced-convection flow subjected to asymmetric thermal conditions. An application to solar thermal collectors. *Sol Energy* 220: 230–245. https://doi.org/10.1016/j.solener.2021.02.022
46. Laube T, Dietrich B, Marocco L, et al. (2022) Turbulent heat transfer in a liquid metal tube flow with azimuthally inhomogeneous heat flux. *Int J Heat Mass Transfer* 189: 122734. https://doi.org/10.1016/j.ijheatmasstransfer.2022.122734
47. Vahidinia F, Khorasanizadeh H, Aghaei A (2021) Comparative energy, exergy and CO_2 emission evaluations of a LS-2 parabolic trough solar collector using Al_2O_3/SiO_2-Syltherm 800 hybrid nanofluid. *Energy Convers Manage* 245: 114596. https://doi.org/10.1016/j.enconman.2021.114596
48. Abed N, Afgan I, Iacovides H, et al. (2021) Thermal-hydraulic analysis of parabolic trough collectors using straight conical strip inserts with nanofluids. *Nanomaterials* 11: 853. https://doi.org/10.3390/nano11040853
49. Fahim T, Laouedj S, Abderrahmane A, et al. (2022) Heat transfer enhancement in parabolic through solar receiver: a three-dimensional numerical investigation. *Nanomaterials* 12: 419. https://doi.org/10.3390/nano12030419
50. Enciso Contreras E, de la Cruz Alejo J, Alcocer GI, et al. (2020) Thermal analysis of a parabolic trough solar collector with synthetic oil as working fluid using a computational tool. *J Technol Prototypes* 6: 1–9. https://doi.org/10.35429/JTP.2020.17.6.1.9

51. Wang Y, Xu J, Liu Q, et al. (2016) Performance analysis of a parabolic trough solar collector using Al_2O_3/synthetic oil nanofluid. *Appl Therm Eng* 107: 469–478. https://doi.org/10.1016/j.applthermaleng.2016.06.170
52. Abubakr M, Amein H, Akoush BM, et al. (2020) An intuitive framework for optimizing energetic and exergetic performances of parabolic trough solar collectors operating with nanofluids. *Renewable Energy* 157: 130–149. https://doi.org/10.1016/j.renene.2020.04.160
53. Akbarimoosavi S, Yaghoubi M (2014) 3D thermal-structural analysis of an absorber tube of a parabolic trough collector and the effect of tube deflection on optical efficiency. *Energy Procedia* 49: 2433–2443. https://doi.org/10.1016/j.egypro.2014.03.258
54. Yaghoubi M, Ahmadi F, Bandehee M (2013) Analysis of heat losses of absorber tubes of parabolic through collector of Shiraz (Iran) solar power plant. *J Clean Energy Technol* 1: 33–37. https://doi.org/10.7763/JOCET.2013.V1.8
55. Fornarelli F, Lippolis A, Oresta P (2017) Buoyancy effect on the flow pattern and the thermal performance of an array of circular cylinders. *J Heat Transfer* 139: 022501. https://doi.org/10.1115/1.4034794
56. Chang C, Li X, Zhang Q (2014) Experimental and numerical study of the heat transfer characteristics in solar thermal absorber tubes with circumferentially non-uniform heat flux. *Energy Procedia* 49: 305–313. https://doi.org/10.1016/j.egypro.2014.03.033
57. White FM, Corfield I (2006) Viscous Fluid Flow. Vol. 3, McGraw-Hill, New York.
58. Menter FR (2009) Review of the shear-stress transport turbulence model experience from an industrial perspective. *In J Comput Fluid Dyn*. 23: 305–316. https://doi.org/10.1080/10618560902773387
59. Malekan M, Khosravi A, Syri S (2019) Heat transfer modeling of a parabolic trough solar collector with working fluid of Fe_3O_4 and CuO/Therminol 66 nanofluids under magnetic field. *Appl Thermal Eng* 163: 114435. https://doi.org/10.1016/j.applthermaleng.2019.114435
60. Hoseinzadeh H, Kasaeian A, Shafii MB (2018) Geometric optimization of parabolic trough solar collector based on the local concentration ratio using the Monte Carlo method. *Energy Convers Manage* 175: 278–287. https://doi.org/10.1016/j.enconman.2018.09.001
61. He YL, Xiao J, Cheng Z, et al. (2011) A MCRT and FVM coupled simulation method for energy conversion process in parabolic trough solar collector. *Renewable Energy* 36: 976–985. https://doi.org/10.1016/j.renene.2010.07.017
62. Agagna B, Smaili A (2021) Effects of rim angle on performance predictions of a parabolic trough solar collector. *Advances in Green Energies and Materials Technology: Selected Articles from the Algerian Symposium on Renewable Energy and Materials (ASREM-2020)*, 375–382. Springer. https://doi.org/10.1007/978-981-16-0378-5_49
63. Mohammed, AK, Talabani ZJ (2013) Study of forced convection heat transfer from horizontal and vertical tubes. *Int J Eng Res Techno* 2: 2011–2017. Available from: https://www.ijert.org/research/study-of-forced-convection-heat-transfer-from-horizontal-and-vertical-tubes-IJERTV2IS100645.pdf.
64. Patankar SV, Spalding DB (1983) A calculation procedure for heat, mass and momentum transfer in three-dimensional parabolic flows. *Numer Predict Flow Heat Transf Turbul Combust*, 54–73. https://doi.org/10.1016/B978-0-08-030937-8.50013-1

65. Jamali H (2016) Analyses of absorber tube of parabolic trough solar collector (PTSC) based on convective heat transfer coefficient of fluid. *Int Energy J* 16: 73–86. Available from: https://www.thaiscience.info/Journals/Article/RIEJ/10992364.pdf.
66. Almanza R, Lentz A, Jimenez G (1997) Receiver behavior in direct steam generation with parabolic troughs. *Sol Energy* 61: 275–278. https://doi.org/10.1016/S0038-092X(97)88854-8
67. Flores V, Almanza R (2004) Behavior of the compound wall copper—steel receiver with stratified two-phase flow regimen in transient states when solar irradiance is arriving on one side of receiver. *Sol Energy* 76: 195–198. https://doi.org/10.1016/j.solener.2003.08.015
68. Wang F, Shuai Y, Yuan Y, et al. (2012) Effects of material selection on the thermal stresses of tube receiver under concentrated solar irradiation. *Mater Des* 33: 284–291. https://doi.org/10.1016/j.matdes.2011.07.048
69. Jamali H (2019) Optimization of thermal efficiency of a parabolic trough solar collector (PTSC) based on new materials application for the absorber tube selective coating and glass cover. *J Appl Res Technol* 16: 384–393. https://doi.org/10.22201/icat.16656423.2018.16.5.742

AIMS Press